



# Two-dimensional covalent organic frameworks as self-template derived nitrogen-doped carbon nanosheets for eco-friendly metal-free catalysis

Xiwei Hu, Yu Long, Mengying Fan, Man Yuan, Hong Zhao, Jiantai Ma, Zhengping Dong\*

State Key Laboratory of Applied Organic Chemistry, Gansu Provincial Engineering Laboratory for Chemical Catalysis, College of Chemistry and Chemical Engineering, Lanzhou University, Lanzhou, 730000, PR China



## ARTICLE INFO

### Keywords:

Covalent organic frameworks  
N-doped mesoporous carbon materials  
Metal-free catalysis  
Hydrogenation of nitroarenes  
Knoevenagel condensation

## ABSTRACT

Heteroatom-doped carbon materials with superior physico-chemical properties and high stability are potential candidates for environmentally friendly metal-free catalysis. In this study, mesoporous carbon materials with high N content and lattice defects were successfully fabricated via self-templated carbonization of a two-dimensional covalent organic framework (2D COF). The ordered structure and clear composition of intrinsic COF precursors aid the understanding of the specific role of dopants in the as-prepared N-doped mesoporous carbon materials. Based on the obtained experimental results and characterizations, graphitic N and its related defects were found to be closely associated with catalytic activity, indicating they are probably the main active sites. In addition, the obtained catalyst showed remarkable catalytic performance in both hydrogenation of nitroarenes and Knoevenagel condensation of aromatic aldehyde derivatives in aqueous solution. This study is expected to provide a new inspiration for the synthesis of heteroatom-doped carbon materials from cost-effective COFs via self-templated carbonization for eco-friendly metal-free catalysis.

## 1. Introduction

Aromatic nitro-compounds as contaminants can be widely found in industrial effluent and have raised urgent concern for human health and environmental protection [1,2]. However, as reduced products of nitroarenes, aromatic amines are important intermediates for the production of dyes, agrochemicals, pharmaceuticals and chelating agents [3–6]. The most environmentally friendly and efficient strategy for transformation of nitroarenes to the more useful corresponding aromatic amines is the catalytic hydrogenation method. Traditionally, the catalytic hydrogenation of nitroarenes involved various metallic catalysts, especially noble-metal catalyst such as Pd [7], Pt [8], Au [9] and Ag [10], and they all exhibited good catalytic performance. Nevertheless, the high price of noble metal and the leaching of noble-metal nanoparticles during the catalytic process are the main drawbacks of these traditional noble-metal catalysts and limit their large-scale applications [11]. Recently, the catalytic hydrogenation of nitroarenes by metal-free catalysts have drawn wide research interest. Gao et al. reported phosphorus-doped and lattice-defective carbon materials as metal-free catalyst for selective hydrogenation of nitroarenes with excellent selectivity (> 99%) [12]. Li et al. reported hierarchical hollow COFs-derived heteroatom doped carbon spheres for metal-free nitroarenes reduction also showed excellent catalytic performance with

almost full conversion and remarkable selectivity [13]. Besides, just as the aromatic amines, benzylidenemalononitrile derivatives that synthesized by Knoevenagel condensation also have extensive application in pesticides, dyes, and optoelectronics [14,15]. Generally, Knoevenagel condensation reaction is catalyzed by weak bases such as amines and pyridine in a homogeneous system [16]. However, the use of toxic solvents and the unsustainability of homogeneous catalysts make the reacting process go against the concept of “Green and Sustainable Chemistry”. Based on the viewpoint of recycling and sustainable development, in recent years, more attentions have been focused on heterogeneous catalysts, such as functionalized graphene oxide supported Rh-Pt nanoparticles [17], MOFs-Pd [18], chitosan [19], carbon doped hexagonal BN [20] etc. However, there are still many deficiencies need to be improved, such as high cost, high temperature, toxic solvent, low selectivity and long reaction time. Therefore, fabrication of novel, cost-effective and stable heterogeneous catalysts with excellent catalytic performance that can be used in both catalytic hydrogenation of nitroarenes and Knoevenagel condensation under environmentally friendly reaction conditions are still urgently needed.

Compared with metal catalysts, carbon materials are environmentally friendly and extremely stable, thus they are ideal candidates to fabricate heterogeneous catalysts [21,22]. However, only using carbon materials as catalysts is rare since the uniform charge

\* Corresponding author.

E-mail address: [dongzhp@lzu.edu.cn](mailto:dongzhp@lzu.edu.cn) (Z. Dong).

distribution and inertness are common properties of all carbon materials, which weakens the interaction between the reactants and the carbon materials. However, when heteroatoms such as N, S, and P were introduced into the carbon matrix, a remarkable catalytic activity of these heteroatom-doped carbon materials could be obtained due to charge delocalization and changes of the electronic structure [12,23–25]. Moreover, doping of the heteroatoms into the carbon matrix can also cause new defects due to the difference in atomic size, bond length, and coordination between carbon atoms and dopants, leading to abundant defect sites with local charge [26,27]. Therefore, the defects caused by heteroatoms doping can serve as active sites and transfer charges to reactants, thus activating the reactants to facilitate catalytic reactions. The above excellent characteristics enable heteroatom-doped carbon materials as perfect metal-free catalysts. Among numerous heteroatom-doped carbon materials, N-doped carbon materials have attracted significant research attention due to abundantly available material sources and excellent catalytic performance. Some N-doped graphitic carbon materials have already been reported for metal-free catalytic applications [28–31].

N-doped carbon materials can be fabricated via various methods such as soft template method [32], hard template method [33], and metal salt-assisted method [34]. All these methods require complex experimental procedures and post-processing operations to introduce heteroatoms into the carbon matrix. Especially, toxic and corrosive acids are usually required during the removal of the template, which are bad for human health and environment [35]. In comparison, self-templated method as a simple and environment-friendly strategy is very suitable for the preparation of heterogeneous catalysts. It's worth mentioning that, covalent organic frameworks (COFs) as a new type of porous material have been intensively investigated for gas storage, catalysis, semiconductors, and adsorption, which are attributed to their high surface area, diverse structural topologies, and tunable compositions [36–38]. They are mainly prepared by using heteroatom-containing precursors, especially N-containing precursors, thus they can act as intrinsic precursors for the fabrication of N-doped carbon materials via facile self-templated methods [39,40]. Moreover, due to their clear compositions and ordered structure of intrinsic COFs precursors, the as-prepared N-doped carbon materials can generally maintain the structure of COFs and can therefore provide more information on the intrinsic role of dopants in metal-free catalysis.

Inspired by the above-mentioned considerations, the present study used the easily available and cheap piperazine and cyanuric chloride to synthesize 2D PC-COF as self-template for preparing N-doped carbon materials (NC-X, X refers to the carbonization temperatures). As expected, the as-prepared NC-700 catalyst exhibit excellent catalytic activity in both hydrogenation of nitroarenes and Knoevenagel condensation in aqueous solution. Based on experimentally obtained results and the analysis of XPS and Raman spectra, graphitic N doping and its related defects in NC catalysts are the critical factors of high catalytic activity. Therefore, this study provides a meaningful platform for the self-templated construction of N-doped carbon materials with excellent catalytic activity and recyclability for environmentally friendly metal-free catalytic applications.

## 2. Experimental section

### 2.1. Materials

Piperazine and cyanuric chloride were purchased from Heowns Biochemical Reagent Co. Ltd. (Tianjin China). Nitroarenes, aromatic aldehydes, hydrazine hydrate and malononitrile were purchased from Sinopharm Chemical Reagent Co. Ltd. (China). All other reagents were of analytical grade and were used without further purification.

### 2.2. Synthesis of PC-COF

Typically, piperazine (12 mmol) and  $K_2CO_3$  (24 mmol) were added into a solution of 1,4-dioxane (100 mL) and cyanuric chloride (8 mmol) in a 250 mL three-necked round flask where the mixture was stirred for 1 h. Then, the reaction mixture was heated to 110 °C for 48 h. After the completion of reaction, the product was isolated by filtration and washed several times with dichloromethane, deionized water, and ethanol, followed by vacuum drying in an oven at 40 °C for 18 h to obtain the PC-COF.

### 2.3. Preparation of NC materials

PC-COF was pyrolyzed at a series of temperatures i.e. 500, 600, 700, and 800 °C for 2 h each, at a heating rate of 2 °C min<sup>-1</sup> under  $N_2$  atmosphere. The resulting black materials were ground to a powder to obtain PC-COF derived N-doped mesoporous carbon materials, which were named as NC-500, NC-600, NC-700, and NC-800, respectively.

### 2.4. Catalytic hydrogenation of nitroarenes

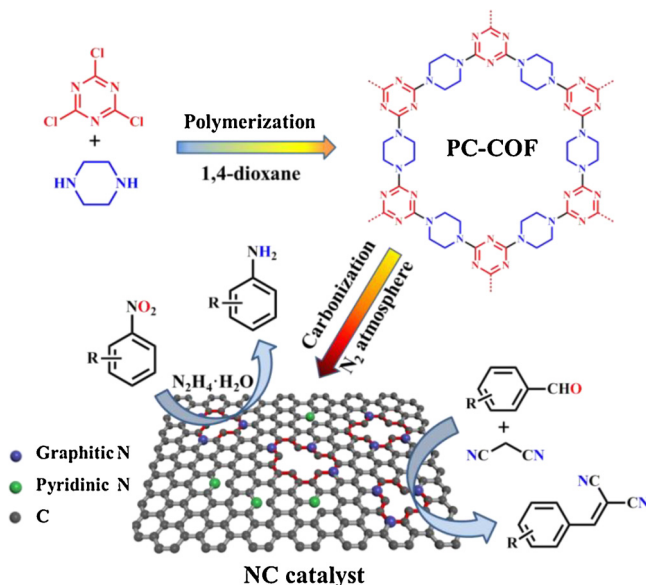
Typically, nitrobenzene (0.5 mmol), hydrazine hydrate (5 mmol), and NC-700 (40 mg) were added into a 25 mL two-neck flask containing 4 mL mixed solvent (ethanol/water, v/v, 1:3) and then stirred at 100 °C. The samples were extracted with ethyl acetate followed by separation of catalyst by filtration. The organic phase was analyzed by gas chromatography-mass spectrometry (GC-MS, Agilent 5977E).

### 2.5. Knoevenagel condensation reaction

Benzaldehyde (1 mmol), malononitrile (1.5 mmol), and NC-700 (20 mg) were added into a 25 mL two-neck flask containing 4 mL mixed solvent (ethanol/water, v/v, 1:3) and stirred at 40 °C. After the reaction, all samples were extracted with ethyl acetate and the catalyst was separated by filtration. The organic phase was analyzed by GC-MS.

### 2.6. Catalyst characterization

Surface morphologies of PC-COF and as-prepared NC materials were observed by transmission electron microscope (TEM, Tecnai G2 F30) and scanning electron microscope (SEM, HITACHI S-4800). Powder X-ray diffraction (PXRD) patterns were obtained on a Rigaku D/max-2400 diffractometer in the range of  $2\theta = 10\text{--}80^\circ$  with Cu- $\kappa\alpha$  radiation. Raman spectra were obtained through a Raman spectrometer (Jobin Yvon Lab Ram HR evolution). X-ray photoelectron spectroscopy (XPS, PHI-5702) was conducted to investigate elemental composition and bonding information of samples. The specific surface areas of the prepared materials were measured by nitrogen adsorption-desorption isotherms at 77 K after degassing the samples using a Micromeritics Model ASAP 2010 instrument. Both the pore size distribution and pore volume were analyzed based on the Barrett-Joyner-Halenda (BJH) method on the desorption branch of the isotherms. The specific surface areas were calculated by Brunauer-Emmett-Teller (BET) method. Fourier transform infrared spectroscopy (FT-IR) spectra were obtained on a Bruker spectrometer (VERTEX 70). The content of C, H, and N elements in catalysts were determined through elemental analysis (EA, CHNS). The reaction conversion and selectivity were determined by GC-MS. Thermogravimetric analysis (TGA) was conducted on a TA-Q50 equipment and the PC-COF was heated from 40 to 900 °C at a heating rate of 10 °C min<sup>-1</sup> under  $N_2$  atmosphere. UV-vis absorption spectra were obtained by an Agilent Cary 5000 UV-vis spectrophotometer.



**Scheme 1.** The preparation procedure and catalytic application of NC catalyst.

### 3. Results and discussion

#### 3.1. Characterization of PC-COF and NC catalysts

PC-COF was synthesized by polymerization of cyanuric chloride and piperazine (Scheme 1). The FT-IR spectra of cyanuric chloride, piperazine, and PC-COF are shown in Fig. 1a. The spectrum of PC-COF shows no indication of the N–H stretching vibration of piperazine at  $3214\text{ cm}^{-1}$  and the C–Cl stretching mode of cyanuric chloride at  $850\text{ cm}^{-1}$ , respectively [36]. In addition, the characteristic framework band at  $806\text{ cm}^{-1}$  indicates the existence of a triazine unit in PC-COF [41]. Furthermore, the existence of the aromatic C=N stretching vibration ( $1550\text{ cm}^{-1}$  for triazinyl C=N), the aromatic C–N stretching vibrations ( $1232\text{ cm}^{-1}$ ,  $1298\text{ cm}^{-1}$ , and  $1365\text{ cm}^{-1}$ ), and the C–H stretching vibrations ( $2850\text{ cm}^{-1}$  and  $2924\text{ cm}^{-1}$ ) of piperazine indicate that both piperazine and triazine units exist in PC-COF [31,42–45]. From the FT-IR spectra results, it can be concluded that PC-COF was successfully synthesized.

TGA analysis shows that PC-COF is thermally stable in the range of  $40\text{ }^\circ\text{C}$  to  $315\text{ }^\circ\text{C}$  (Fig. 1b). When heated from  $315\text{ }^\circ\text{C}$  to  $513\text{ }^\circ\text{C}$ , a weight loss of 47.7% was occurred which is attributed to the thermal decomposition of PC-COF, and this process completes the transformation of PC-COF to NC material. The weight loss of 35.6% during the heating from  $513\text{ }^\circ\text{C}$  to  $900\text{ }^\circ\text{C}$  is the result of the further pyrolysis of NC material, which is accompanied by the loss of C and N-containing groups in

its framework.

The morphologies of PC-COF and as-prepared NC materials were investigated via SEM and TEM images. The PC-COF has a spherical morphology as shown in Fig. 2a. The SEM images of NC materials show a similar spherical morphology. The spherical particles in NC materials are smaller and more uniform in size distribution, which may be due to the dimension shrinkage during carbonization (Fig. 2b, Fig. S1). In addition, a stacking layered morphology and a porous structure can be observed in the TEM image of PC-COF due to the stacking of 2D sheets (Fig. 2c). As shown in Fig. 2d, the TEM image of NC-700 shows an unchanged stacking layered morphology and porous structure compared to that of PC-COF, which may contribute to the structural stability of PC-COF. It is obvious that the as-prepared NC materials retain the original morphology of PC-COF, benefiting from the self-templated carbonization method. The elemental mapping images of NC-700 indicate that N atoms are evenly distributed in the mesoporous carbon layer (Fig. 2e), which is the result of both the triazinyl and piperazine units in the PC-COF framework.

The nitrogen adsorption-desorption isotherm shows that the surface area of PC-COF is  $601.4\text{ m}^2\text{ g}^{-1}$  and the corresponding pore size distribution curve shows that the average pore size of PC-COF is centered at  $3.7\text{ nm}$  (Fig. S2). In addition, the nitrogen adsorption-desorption isotherms (Fig. 3a) of all NC catalysts show type IV isotherms with hysteresis loops from  $P/P_0 = 0.45$  to  $1.0$ , indicating a highly uniform mesoporous structure in NC materials [46,47]. Moreover, the corresponding pore size distribution curves display the distribution of small mesopores centered at  $4.5\text{ nm}$  (Fig. 3b), further illustrating the uniform distribution of mesoporous structures in all NC materials. In addition, NC-700 has the lowest specific surface area ( $52.4\text{ m}^2\text{ g}^{-1}$ ), the smallest pore volume ( $0.20\text{ cm}^3\text{ g}^{-1}$ ), and the largest average pore size ( $15.5\text{ nm}$ ) (Table S1, entry 3). In contrast, the highest specific surface area ( $253.6\text{ m}^2\text{ g}^{-1}$ ), the largest pore volume ( $0.39\text{ cm}^3\text{ g}^{-1}$ ), and smallest average pore size ( $6.2\text{ nm}$ ) were found in NC-800 (Table S1, entry 4).

The PXRD pattern shows that PC-COF is a crystalline polymer with five main peaks at  $12.7^\circ$ ,  $28.3^\circ$ ,  $29.6^\circ$ ,  $32.6^\circ$ , and  $41.6^\circ$  (Fig. S3). Compared to that of PC-COF, the PXRD patterns of prepared NC catalysts show that all distinct peaks disappear but exhibit only one broad peak at around  $25^\circ$  (Fig. 4a), which is indexed to the (002) plane of graphitic carbon [48]. Moreover, for NC-600, NC-700 and NC-800, the intensity of peaks at  $25^\circ$  in Fig. 4a are stronger than that of NC-500, indicating the increase in degree of graphitization from NC-500 to NC-800. As shown in the Raman spectra (Fig. 4b), two characteristic peaks at around  $1335\text{ cm}^{-1}$  and  $1592\text{ cm}^{-1}$  correspond to the D and G bands, which refer to the lattice defects and the graphitic phase, respectively [49,50]. Hence, the relative intensity of two peaks ( $I_D/I_G$ ) represents the density of defects in the materials. The values of  $I_D/I_G$  increased from 1.01 to 1.13 with an increase in pyrolysis temperature from  $500\text{ }^\circ\text{C}$  to  $700\text{ }^\circ\text{C}$ , while it decreased to 0.91 when the pyrolysis temperature

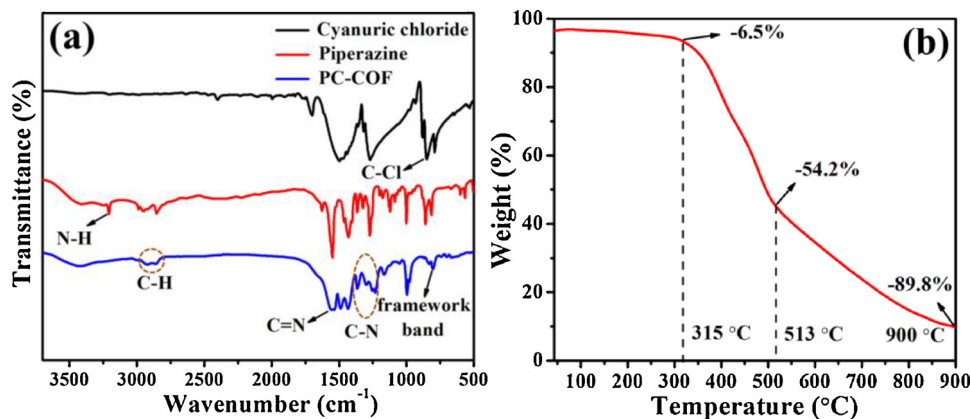


**Fig. 1.** (a) FT-IR spectra of cyanuric chloride, piperazine and PC-COF. (b) TGA curve of PC-COF.

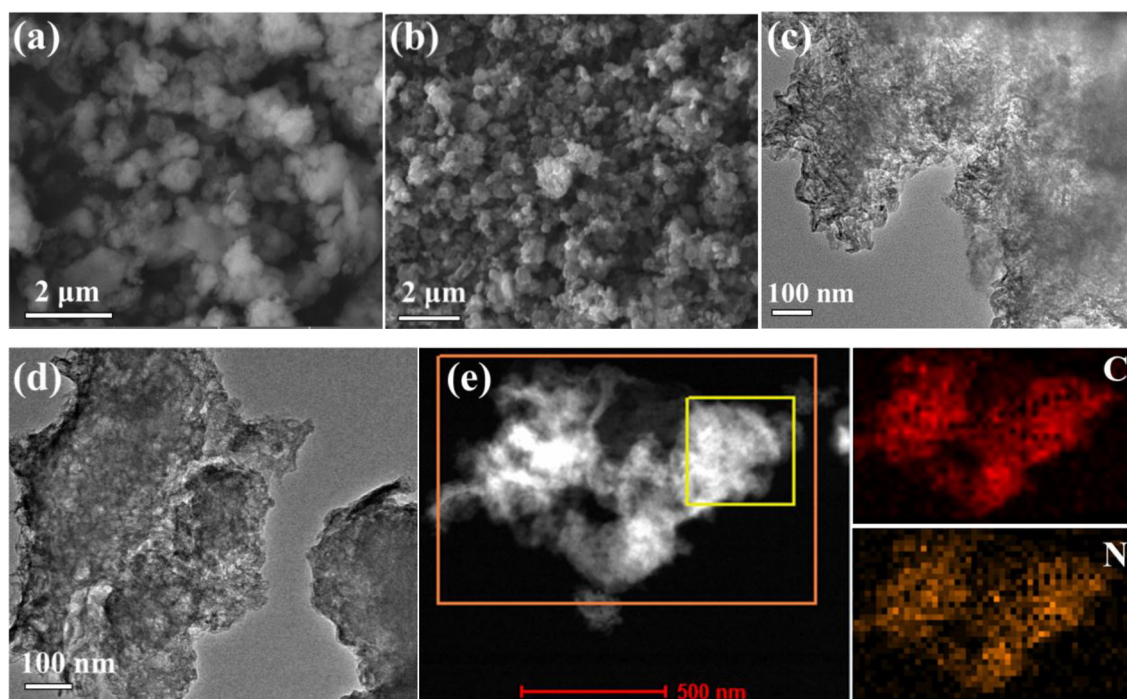


**Fig. 2.** SEM images of PC-COF (a) and NC-700 (b); TEM images of PC-COF (c) and NC-700 (d); EDX mapping images (e) of NC-700 for C and N elements.

increased to 800 °C. Thus, NC-700 showed the highest  $I_D/I_G$  value, suggesting its matrix contains the highest concentration of defects.

XPS was performed to determine the chemical elements present in the NC catalysts and to explain the possible cause of defect formation. Based on the XPS wide scan spectra, all of the NC catalysts were found to contain C, N, and O elements (Fig. 5a), which was also confirmed by the EDX spectrum (Fig. S4). Based on Fig. S5, the high-resolution C 1 s XPS spectra of NC catalysts show peaks at 284.4–284.6 eV, 285.5–285.9 eV, 286.4–286.9 eV, and 288.7–290.0 eV, corresponding to  $\text{sp}^2$ -hybridized C=C, C=N, C–N, and O–C=O, respectively [51–56]. The existence of C–N and C=N in the C 1 s spectra confirms that N atoms have been successfully embedded in the lattice of carbon. An identical feature can also be found in Fig. 5b, which shows the existence of both pyridinic N (398.1–398.2 eV) and graphitic N (400.8–401.3 eV) in the N 1 s spectra of NC catalysts [57,58].

### 3.2. Study of the defect formation of NC catalysts

As shown in Table 1, the N contents determined by chemical element analysis in all NC catalysts, show a decreasing trend with the increase of pyrolysis temperature (from 500 °C to 800 °C). Similarly, the

N contents of NC catalysts determined by XPS wide scan spectra show the same trend. Furthermore, to ascertain the cause of defect formation, the information of different N species in each NC catalyst was also analyzed based on high-resolution N 1 s spectra. From NC-500 to NC-800, the percentages of graphitic N in the corresponding NC catalysts show an increasing trend (Fig. 5c). Moreover, the exact graphitic N content in each NC catalyst, which is calculated based on the XPS N contents and the percentages of graphitic N in their high-resolution N 1 s spectra, show a similarly increasing trend with the increase of pyrolysis temperature except for NC-800 (Table 1, entries 1–4). Although the highest percentage of graphitic N was found in NC-800, the calculated graphitic N content is the lowest (Fig. 5c and Table 1, entry 4). This may be attributed to the significant loss of N atoms at high pyrolysis temperature, leading to a dramatic decrease in the overall N content of NC-800.

Based on the results above, the values of  $I_D/I_G$  are approximately linear with the concentration of graphitic N in NC-500, NC-600, and NC-700 (Fig. S6a), indicating that the formation of defects in the lattice of carbon should be attributed to graphitic N doping. For NC-800, a significant loss of N atoms during deep carbonization results in a low concentration of graphitic N atoms in the lattice of carbon, which leads

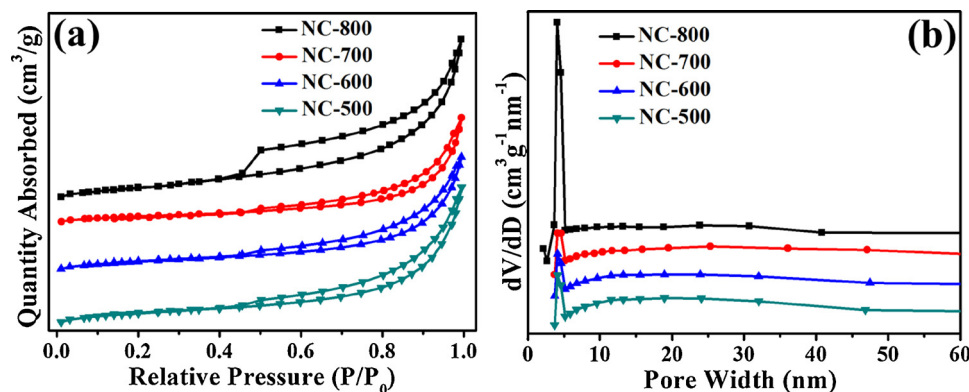


**Fig. 3.** Nitrogen adsorption-desorption isotherms (a) and the corresponding pore size distribution curves (b) of NC-500, NC-600, NC-700 and NC-800.

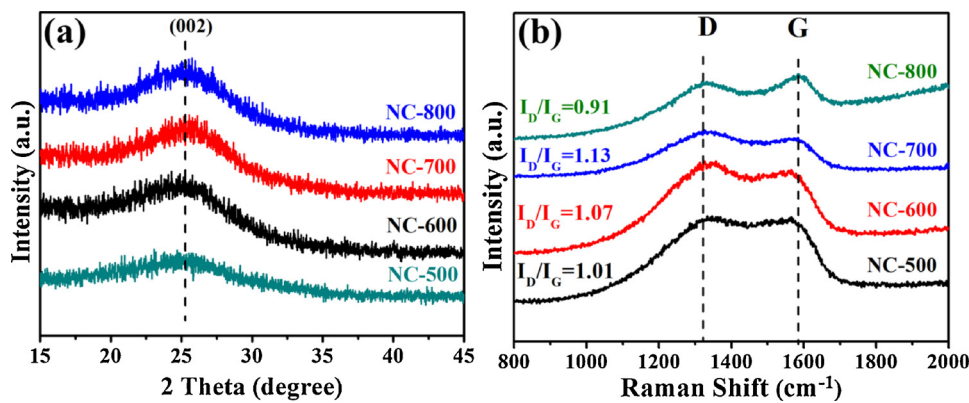


Fig. 4. XRD patterns (a) and Raman spectra (b) of NC-500, NC-600, NC-700 and NC-800.

to the lowest  $I_D/I_G$  ratio, further causing the value of  $I_D/I_G$  in NC-800 is not linear with concentration of graphitic N in NC-800 anymore. It is worth to mention that, NC-800 was obtained under maximal pyrolysis temperature, while possesses the lowest value of  $I_D/I_G$ , which confirms that the formation of defects is the result of graphitic N doping rather than high pyrolysis temperature.

### 3.3. Screening of reaction conditions for hydrogenation of nitroarenes

As illustrated in Table 2, various factors were taken into account, such as the amount of catalyst, volume ratios of ethanol to water, reaction temperature and the concentration of  $N_2H_4\cdot H_2O$ . The conversion of nitrobenzene exceeds 99% when the catalyst amount is 40 mg, while it becomes lower when the amount decreased to 30 mg and remains almost unchanged when the amount increased to 50 mg (Table 2, entries 4–6). In addition, the effect of different volume ratios of ethanol to water on the reaction activity was investigated with NC-700 as catalyst. All volume ratios of ethanol to water showed excellent activity with high conversion of nitrobenzene (> 95%) and selectivity to aniline (> 99%) (Table 2, entries 4, 7–10). Although ethanol and a mixed

Table 1

The element contents obtained from chemical element analysis and XPS analysis in NC catalysts.

Entry	Catalyst	EA	XPS		
			N [wt. %]	N [at. %]	Pyridinic N [at. %]
1	NC-500	30.7	24.7	14.6	10.1
2	NC-600	28.8	24.3	14.0	10.3
3	NC-700	23.0	17.3	6.7	10.5
4	NC-800	5.2	4.5	1.6	2.9

solvent (ethanol/water, v/v, 1:3) showed equally excellent catalytic performance for the hydrogenation of nitrobenzene, the latter was chosen as reaction solvent due to the environmental friendliness and the inexpensive nature of water. Moreover, a higher reaction temperature is conducive for the improvement of the conversion of nitrobenzene. A significant decrease in the conversion occurred at lower reaction temperatures (Table 2, entries 9 and 11–13). With increasing  $N_2H_4\cdot H_2O$  concentration, the reactivity showed an increasing trend and

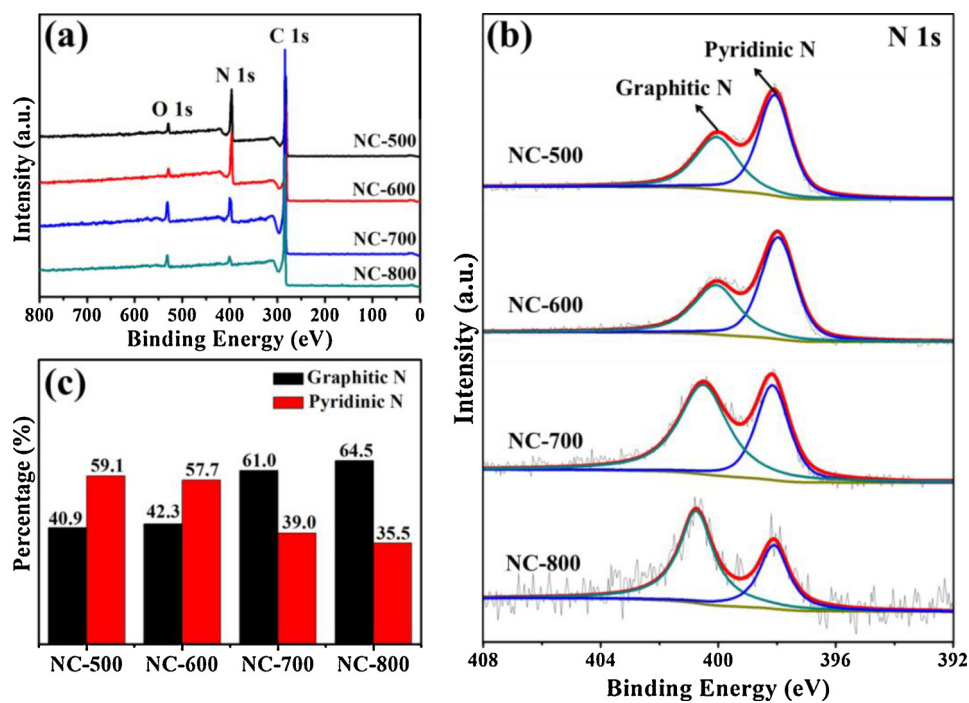


Fig. 5. XPS wide scan spectra (a) and high-resolution N 1 s spectra (b) of as-prepared NC catalysts. (c) The percentages of graphitic N and pyridinic N in NC-500, NC-600, NC-700 and NC-800.

**Table 2**The optimization of reaction conditions for hydrogenation of nitrobenzene.<sup>a</sup>

Entry	Catalyst/mg	Solvent	Temp. (°C)	Time (h)	Conv./Sel. (%)	TOF (mol·g <sup>-1</sup> h <sup>-1</sup> ) <sup>b</sup>
1	NC-500/40	Ethanol	100	3.5	43.8/ > 99	$1.56 \times 10^{-3}$
2	NC-600/40	Ethanol	100	3.5	77.8/ > 99	$2.78 \times 10^{-3}$
3	NC-800/40	Ethanol	100	3.5	98.8/ > 99	$3.53 \times 10^{-3}$
4	NC-700/40	Ethanol	100	3.5	> 99/ > 99	$3.57 \times 10^{-3}$
5	NC-700/30	Ethanol	100	3.5	73.7/ > 99	$3.51 \times 10^{-3}$
6	NC-700/50	Ethanol	100	3.5	98.7/ > 99	$2.82 \times 10^{-3}$
7	NC-700/40	E:W = 3:1	100	3.5	97.6/ > 99	$3.49 \times 10^{-3}$
8	NC-700/40	E:W = 2:2	100	3.5	96.3/ > 99	$3.44 \times 10^{-3}$
9	NC-700/40	E:W = 1:3	100	3.5	> 99/ > 99	$3.57 \times 10^{-3}$
10	NC-700/40	Water	100	3.5	95.2/ > 99	$3.40 \times 10^{-3}$
11	NC-700/40	E:W = 1:3	80	3.5	76.5/ > 99	$2.73 \times 10^{-3}$
12	NC-700/40	E:W = 1:3	50	3.5	17.4/ > 99	$6.21 \times 10^{-4}$
13	NC-700/40	E:W = 1:3	25	3.5	6.0/ > 99	$2.14 \times 10^{-4}$
14 <sup>b</sup>	NC-700/40	E:W = 1:3	100	3.5	92.8/ > 99	$3.31 \times 10^{-3}$
15 <sup>c</sup>	NC-700/40	E:W = 1:3	100	3.5	90.3/ > 99	$3.23 \times 10^{-3}$
16 <sup>d</sup>	NC-700/40	E:W = 1:3	100	7	0.6/ > 99	–
17 <sup>e</sup>	NC-700/40	E:W = 1:3	100	3.5	66.0/ > 99	$2.36 \times 10^{-3}$
18 <sup>f</sup>	NC-700/40	E:W = 1:3	100	3.5	5.5/ > 99	$1.96 \times 10^{-4}$
19 <sup>g</sup>	NC-700/40	E:W = 1:3	100	3.5	5.1/ > 99	$1.82 \times 10^{-4}$
20 <sup>h</sup>	NC-700/40	E:W = 1:3	100	3.5	1.3/ > 99	–
21	Graphite powder	E:W = 1:3	100	3.5	30.2/ > 99	$1.08 \times 10^{-3}$
22	CNTs	E:W = 1:3	100	3.5	27.7/ > 99	$9.89 \times 10^{-4}$
23	g-C <sub>3</sub> N <sub>4</sub>	E:W = 1:3	100	3.5	42.5/ > 99	$1.52 \times 10^{-3}$
24	PC-COF	E:W = 1:3	100	3.5	5.9/ > 99	$2.11 \times 10^{-4}$
25	none	E:W = 1:3	100	7	1.2/ > 99	–

<sup>a</sup> Reaction conditions: 0.5 mmol substrate, 5 mmol hydrazine hydrate, 40 mg catalyst, 4 mL solvent, unless otherwise mentioned. <sup>b</sup> 3 mmol N<sub>2</sub>H<sub>4</sub>·H<sub>2</sub>O. <sup>c</sup> 1 mmol N<sub>2</sub>H<sub>4</sub>·H<sub>2</sub>O. <sup>d</sup> Without N<sub>2</sub>H<sub>4</sub>·H<sub>2</sub>O. <sup>e</sup>, <sup>f</sup>, <sup>g</sup>, <sup>h</sup> Using NaBH<sub>4</sub>, formic acid, isopropanol and H<sub>2</sub> as hydrogen donors, respectively. The conversion and selectivity were determined by GC-MS. <sup>b</sup> Turnover frequency (TOF) =  $\frac{\text{mole of converted substrate}}{\text{g catalyst} \times \text{h reaction time}}$ .

then reached the highest point when the concentration reached 5 mmol (Table 2, entries 9, 14 and 15). Different hydrogen donors, such as formic acid, NaBH<sub>4</sub>, isopropanol, and H<sub>2</sub> were also tested. However, only NaBH<sub>4</sub> showed obvious reducing activity, which was lower than that of N<sub>2</sub>H<sub>4</sub>·H<sub>2</sub>O (Table 2, entries 9, 17-20), others showed no significant effect. Thus, N<sub>2</sub>H<sub>4</sub>·H<sub>2</sub>O was selected herein as an ideal reductant, not only due to its excellent reaction activity, but also because it only decomposes into water and nitrogen after the reaction. Moreover, TOF values were calculated to further determine the optimal reaction conditions, based on the calculated result, the hydrogenation reaction proceeded with 40 mg NC-700 catalyst in the presence of 5 mmol N<sub>2</sub>H<sub>4</sub>·H<sub>2</sub>O showed the highest TOF value ( $3.57 \times 10^{-3}$  mol·g<sup>-1</sup> h<sup>-1</sup>) and also the best catalytic performance (Table 2, entry 4). In addition, NC-700 shows competitive catalytic activity in comparison to similar materials, such as graphite powder, CNTs, and g-C<sub>3</sub>N<sub>4</sub>, under identical reaction conditions (Table 2, entries 21-23). If PC-COF was used as catalyst, a very low conversion (5.9%) of nitrobenzene was observed (Table 2, entry 24). Moreover, the reaction proceeded without hydrogen donors or catalysts will lead to poor conversion of nitrobenzene (Table 2, entries 16 and 25).

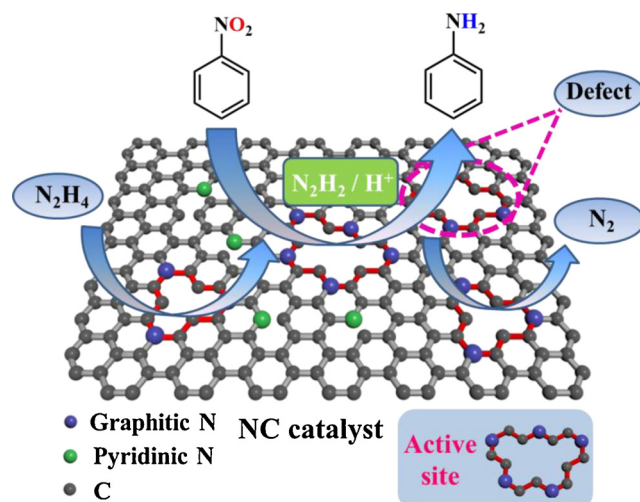
### 3.4. Analysis of active sites and reaction mechanism for catalytic hydrogenation of nitroarenes

Compared to NC-500, NC-600, and NC-800, the NC-700 catalyst with the highest concentration of graphitic N atoms and defects shows the highest conversion (> 99%) and selectivity (> 99%) and also the maximum TOF value ( $3.57 \times 10^{-3}$  mol·g<sup>-1</sup> h<sup>-1</sup>) (Table 2, entries 1-4). Notably, the yield of aniline changes linearly with the content of graphitic N atoms and/or the values of  $I_D/I_G$  in NC-500, NC-600, and NC-700 (Fig. S6b), while it is not directly correlated to the surface area of the above catalysts (Table S1, entries 1-4). Thus it can be concluded that the formation of defects resulting from graphitic N doping, instead of surface area, is the key to the high catalytic performance. In addition,

although NC-800 possesses the lowest defect density and graphitic N content, it shows unexpectedly good catalytic performance (Table 2, entry 3). This may be attributed to its surface area which is much larger than that of other NC catalysts (Table S1, entry 4) and thus can provide more accessible active sites with a constant amount of catalyst. By analyzing the difference between NC-800 and other NC catalysts, it also can be concluded that only when specific surface area reaches a specific high value will the reaction be promoted.

N-doping and the formation of nitrogen-related defects proved to be effective in improving the catalytic performance of carbon materials. Wu et al. reported that N-doping equips N-doped CNTs with higher electrocatalytic activity than Pt, as a result of the introduction of high density of positive charge to the carbon atoms adjacent to N-dopants [59]. Additionally, the nitrogen-related defects may lead to a metallic nature of the carbon materials [60]. Therefore, the NC materials in this study are expected to have a similarly excellent performance in electronic transmissions, which can benefit the activation of N<sub>2</sub>H<sub>4</sub> and the nitro group for nitroarenes hydrogenation. Based on the present facts and the experimentally obtained results, the possible mechanism of hydrogenation of nitrobenzene with N<sub>2</sub>H<sub>4</sub>·H<sub>2</sub>O is illustrated in Scheme 2. The adsorbed N<sub>2</sub>H<sub>4</sub> on the surface of the NC catalyst was decomposed to N<sub>2</sub>H<sub>2</sub> accompanied by the formation of two electrons and two protons. The generated N<sub>2</sub>H<sub>2</sub> and/or protons are expected to attack the -NO<sub>2</sub> of nitrobenzene absorbed locally around the defects and graphitic N atoms. The hydrogenation of nitrobenzene to aniline is completed through the above-mentioned process.

As shown in Fig. 6a, the concentrations of nitrobenzene and aniline change linearly with reaction time, suggesting that the hydrogenation of nitrobenzene on NC-700 catalyst accords with pseudo-zero-order kinetics. This is quite different from the reported metallic catalysts, which accord with pseudo-first-order kinetics [61–63]. Therefore, a series of related experiments were conducted to further corroborate this finding. As shown in Fig. 6b, the concentration of aniline varies linearly with the reaction time, and the slope of the lines increases with the



**Scheme 2.** A possible reaction mechanism for the hydrogenation of nitrobenzene catalyzed by NC catalyst with the existence of  $\text{N}_2\text{H}_4\cdot\text{H}_2\text{O}$ .

increasing amount of NC-700 catalyst. Moreover, the slope of the lines is constant with the increasing concentration of nitrobenzene, as illustrated in Fig. 6c and d. The results of these experiments indicate that the reaction rate of hydrogenation of nitrobenzene catalyzed by NC-700 is determined by the concentration of active sites on NC catalysts rather than the concentration of nitrobenzene. Thus, the fact that nitrobenzene hydrogenation on the NC-700 catalyst accords with the pseudo-zero-order kinetics was further confirmed. Additionally, the faster rate of substrate adsorption, compared to its desorption has been considered as the critical factor leading to pseudo-zero-order kinetics [29]. Therefore, the adsorption experiment of 4-nitrophenol on NC-700 was conducted to prove the rapid adsorption of substrate. The adsorption process was monitored by a UV-vis spectrophotometer at regular intervals. As illustrated by the UV-vis absorption spectra (Fig. S7a), the intensity of the peak at 317 nm decreases sharply during the first 0.5 h and then

gradually decreases, which proves efficient adsorption of 4-nitrophenol on NC-700. Moreover, the strong adsorption of substrate on NC-700 was further illustrated by the FT-IR spectra. As shown in Fig. S7b, the existence of symmetric and asymmetric stretching vibrations of the nitro group at  $1342\text{ cm}^{-1}$  and  $1533\text{ cm}^{-1}$  after adsorption of nitrobenzene demonstrated the strong adsorption of  $-\text{NO}_2$  on NC-700 [64].

### 3.5. Catalytic activity test in hydrogenation of substituted nitroarenes

As shown in Table 3, the catalytic activity in hydrogenation of various substituted nitroarenes was investigated under optimal reaction conditions using the NC-700 catalyst. Firstly, the hydrogenation of halogenated nitroarenes was investigated. For the ortho-substituted and para-substituted substrates show higher conversion, while the selectivity to corresponding aromatic amines is lower than that of meta-substituted nitrobenzene (Table 3, entries 1–3). Similarly, 2-Bromonitrobenzene exhibits higher conversion and lower selectivity to corresponding aromatic amine compared to 3-Bromonitrobenzene (Table 3, entries 4–5). Additionally, a slight dehalogenation occurred in the hydrogenation of halogenated nitroarenes (Table 3, entries 1–6), which is also a common phenomenon for noble metal catalysts [65,66]. Secondly, the hydrogenation of nitroarenes with electron-donating groups was also studied. All of the nitrobenzenes substituted with a methyl group, show almost full conversion and excellent selectivity (Table 3, entries 7–9). Other electron-donor groups such as  $-\text{NH}_2$  and  $-\text{OH}$  also showed excellent performance in conversion and selectivity in a longer reaction time (Table 3, entries 10–14). Moreover, the substituted nitrobenzene with both electron-withdrawing and electron-donating groups show high conversion as well as selectivity (Table 3, entries 15). From the results above, the NC-700 catalyst exhibits excellent catalytic performance in the hydrogenation of various substituted nitroarenes.

### 3.6. Knoevenagel condensation catalyzed by NC-700 catalyst

Knoevenagel condensation was conducted in a mixed solvent

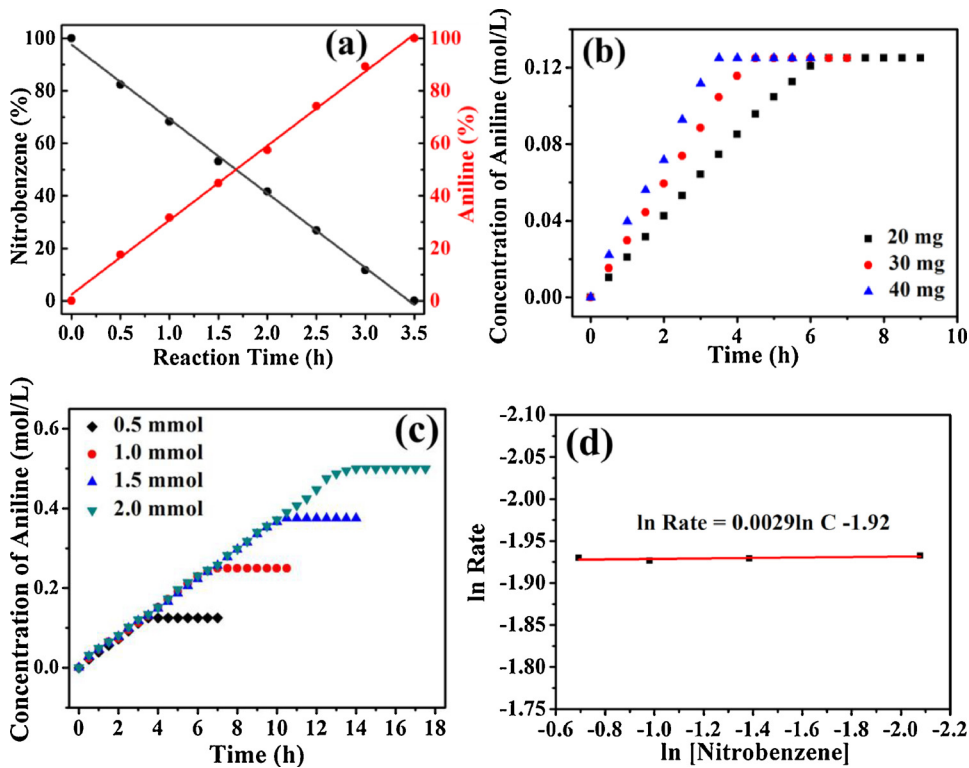


**Fig. 6.** (a) Kinetic profile of nitrobenzene hydrogenation to aniline using NC-700 catalyst. Reaction conditions: 0.5 mmol nitrobenzene, 5 mmol  $\text{N}_2\text{H}_4\cdot\text{H}_2\text{O}$ , 40 mg NC-700, 4 mL of ethanol/water (v/v, 1:3),  $100\text{ }^\circ\text{C}$ . (b) Plots of concentration of aniline versus reaction time for the hydrogenation of nitrobenzene catalyzed by different amount of NC-700 catalyst. Reaction conditions: 0.5 mmol nitrobenzene, 5 mmol  $\text{N}_2\text{H}_4\cdot\text{H}_2\text{O}$ , 4 mL of ethanol/water (v/v, 1:3),  $100\text{ }^\circ\text{C}$ . (c) Plots of concentration of aniline versus reaction time obtained by using different concentrations of nitrobenzene. Reaction conditions: 5 mmol  $\text{N}_2\text{H}_4\cdot\text{H}_2\text{O}$ , 40 mg NC-700, 4 mL of ethanol/water (v/v, 1:3),  $100\text{ }^\circ\text{C}$ . (d) Plot of reaction rate versus the concentration of nitrobenzene (both in logarithmic scale).

**Table 3**The hydrogenation of different nitroarenes on NC-700 under optimal condition.<sup>a</sup>

Entry	Substrate	Product	Time (h)	Conv. (%) <sup>b</sup>	Sel. (%) <sup>b</sup>	TOF (mol·g <sup>-1</sup> h <sup>-1</sup> )
1			2	100	90.8	$5.68 \times 10^{-3}$
2			2	99.5	93.0	$5.78 \times 10^{-3}$
3			2.5	100	83.2	$4.16 \times 10^{-3}$
4			2.5	100	87.9	$4.40 \times 10^{-3}$
5			2.5	99.6	94.2	$4.69 \times 10^{-3}$
6			3.5	100	96.6	$3.45 \times 10^{-3}$
7			3.5	100	> 99	$3.57 \times 10^{-3}$
8			3.5	99.0	> 99	$3.54 \times 10^{-3}$
9			3.5	100	> 99	$3.57 \times 10^{-3}$
10			5	100	> 99	$2.50 \times 10^{-3}$
11			7	98.6	> 99	$1.76 \times 10^{-3}$
12			10	100	> 99	$1.25 \times 10^{-3}$
13			12	100	> 99	$1.04 \times 10^{-3}$
14			15	100	> 99	$8.33 \times 10^{-4}$
15			3.5	96.3	> 99	$3.44 \times 10^{-3}$

<sup>a</sup> Reaction conditions: 0.5 mmol substrate, 5 mmol N<sub>2</sub>H<sub>4</sub>·H<sub>2</sub>O, 40 mg NC-700, 4 ml of ethanol/water (v/v, 1:3), 100 °C.<sup>b</sup> Conversion and selectivity were determined by GC-MS.

ethanol/water (v/v, 1:3) at 40 °C to further expand the applied range and test the catalytic activity of NC-700 catalyst. As a result, benzylidenemalononitrile was successfully synthesized with almost full conversion and excellent selectivity within 1 h under mild conditions (**Table 4, entry 1**). Additionally, as shown in **Table 4**, almost all aryl aldehyde derivatives, whether with electron-withdrawing or electron-donating groups, were successfully converted to the corresponding products with high conversion and excellent selectivity in a relatively short reaction time (**Table 4, entries 2–8**). The exceptions are 3-methylbenzaldehyde and 3,4-dimethylbenzaldehyde, which needed a longer reaction time due to the strong electron-donating effect (**Table 4, entries 9–10**). It is worth noting that furaldehyde and its derivative were also efficiently transformed into corresponding products achieving almost full conversion and high selectivity (**Table 4, entries 11–12**). Thus, it can be concluded that, NC-700 acts as a versatile catalyst in both hydrogenation reaction and Knoevenagel condensation.

### 3.7. Recycling performance of NC-700 in hydrogenation of nitrobenzene and Knoevenagel condensation

The recyclability and stability as important evaluation factors of the catalytic performance of heterogeneous catalysts were tested in the hydrogenation of nitrobenzene and Knoevenagel condensation reaction. As shown in **Fig. 7a and b**, no obvious decrease in conversion and selectivity was found even after eight cycles in the both reactions, suggesting the excellent recyclability of NC-700. A series of characterizations of reused NC-700 was conducted to further confirm the stability of NC-700. The TEM image of reused NC-700 shows the same stacking layered morphology and porous structure as fresh NC-700

(**Fig. S8**), suggesting structural stability of NC-700 during the reaction. The elemental composition and bonding configurations of reused NC-700 were analyzed by both FT-IR (**Fig. S9**) and XPS spectra (**Fig. S10**). They remain nearly unchanged after eight cycles, suggesting that NC-700 has excellent chemical stability. In addition, the PXRD pattern (**Fig. S11**) of reused NC-700 shows unchanged peaks compared to that of fresh catalyst. The above characterizations clearly demonstrate the outstanding recyclability and stability of the NC-700 catalyst.

### 4. Conclusions

NC materials with abundant N atoms and lattice defects were successfully fabricated via self-templated carbonization of a 2D PC-COF. Due to the abundant N atoms and lattice defects in the framework of NC-700 catalyst, the remarkable catalytic performance in both hydrogenation of nitroarenes and Knoevenagel condensation of aromatic aldehyde derivatives in aqueous solution have been well demonstrated. Based on experimentally obtained results and a series of related characterizations, it can be concluded that graphitic N doping and its related defects in NC catalysts are the critical factors of high catalytic activity. Moreover, the hydrogenation of nitroarenes on NC-700 follows pseudo-zero-order kinetics, which differs from the reported pseudo-first-order kinetics followed by the reactions catalyzed by metallic catalysts. In addition, due to the remarkable structural stability of PC-COF, it derived NC-700 catalyst displayed no obvious decrease in conversion and selectivity in both hydrogenation of nitrobenzene and Knoevenagel condensation reaction even after eight reaction cycles. This work is expected to offer a new inspiration for the synthesis of N-doped mesoporous carbon materials from 2D COFs via self-templated

**Table 4**The Knoevenagel condensation of aromatic aldehyde derivatives on NC-700.<sup>a</sup>

Entry	Substrate	Product	Time (h)	Conv. (%) <sup>b</sup>	Sel. (%) <sup>b</sup>	TOF (mol·g <sup>-1</sup> h <sup>-1</sup> )
1	<chem>c1ccccc1CHO</chem>	<chem>c1ccccc1C=CC#N</chem>	1	> 99	> 99	$5.0 \times 10^{-2}$
2	<chem>Fc1ccccc1CHO</chem>	<chem>Fc1ccccc1C=CC#N</chem>	0.75	> 99	> 99	$6.7 \times 10^{-2}$
3	<chem>Clc1ccccc1CHO</chem>	<chem>Clc1ccccc1C=CC#N</chem>	1	> 99	> 99	$5.0 \times 10^{-2}$
4	<chem>Brc1ccccc1CHO</chem>	<chem>Brc1ccccc1C=CC#N</chem>	1.5	> 99	> 99	$3.3 \times 10^{-2}$
5	<chem>O=[N+]([O-])c1ccccc1CHO</chem>	<chem>O=[N+]([O-])c1ccccc1C=CC#N</chem>	1	> 99	> 99	$5.0 \times 10^{-2}$
6	<chem>Oc1ccccc1CHO</chem>	<chem>Oc1ccccc1C=CC#N</chem>	1.5	> 99	> 99	$3.3 \times 10^{-2}$
7	<chem>Oc1cc(O)c(cc1)CHO</chem>	<chem>Oc1cc(O)c(cc1)C=CC#N</chem>	1.5	> 99	> 99	$3.3 \times 10^{-2}$
8	<chem>Oc1cc(Oc2ccccc2)cc1CHO</chem>	<chem>Oc1cc(Oc2ccccc2)cc1C=CC#N</chem>	1.5	> 99	> 99	$3.3 \times 10^{-2}$
9	<chem>Cc1ccccc1CHO</chem>	<chem>Cc1ccccc1C=CC#N</chem>	3	> 99	> 99	$1.7 \times 10^{-2}$
10	<chem>C(C)c1ccccc1CHO</chem>	<chem>C(C)c1ccccc1C=CC#N</chem>	4	98.6	> 99	$1.2 \times 10^{-2}$
11	<chem>O=C1OC(F)=CC1</chem>	<chem>O=C1OC(F)=CC1C=CC#N</chem>	1	> 99	> 99	$5.0 \times 10^{-2}$
12	<chem>OCC1OC(F)=CC1</chem>	<chem>OCC1OC(F)=CC1C=CC#N</chem>	1	> 99	95.7	$4.8 \times 10^{-2}$

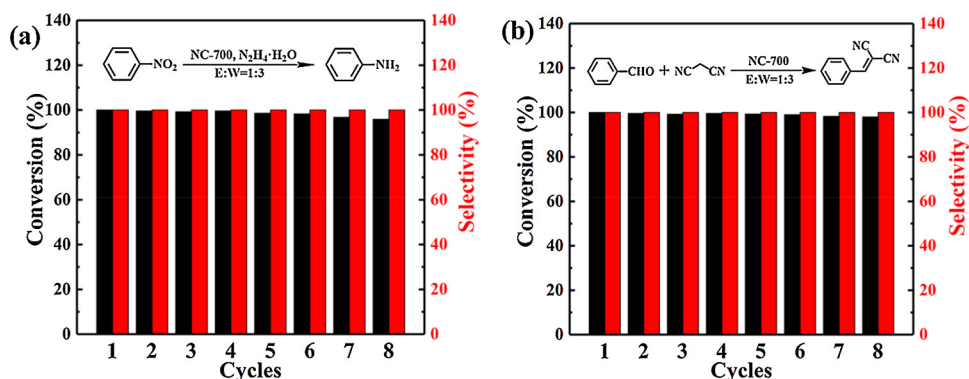
<sup>a</sup> Reaction conditions: 1 mmol substrate, 1.5 mmol malononitrile, 20 mg NC-700, 4 mL of ethanol/water (v/v, 1:3), 40 °C.<sup>b</sup> Conversion and selectivity were determined by GC-MS.

Fig. 7. Recycling performance of NC-700 catalyst in hydrogenation of nitrobenzene (a) and Knoevenagel condensation (b).

method for eco-friendly metal-free catalysis. Furthermore, the relationship between the different nitrogen species and catalytic activity has been clarified.

### Acknowledgement

We thank the financial support from the Fundamental Research Funds for the Central Universities (Izujbky-2017-112).

### Appendix A. Supplementary data

Supplementary material related to this article can be found, in the online version, at doi:<https://doi.org/10.1016/j.apcatb.2018.11.028>.

### References

- [1] S. Giri, R. Das, C. van der Westhuyzen, A. Maity, An efficient selective reduction of nitroarenes catalyzed by reusable silver-adsorbed waste nanocomposite, *Appl. Catal. B: Environ.* 209 (2017) 669–678.

- [2] S. Dayan, F. Arslan, N. Kalaycioglu Ozpozan, Ru(II) impregnated  $\text{Al}_2\text{O}_3$ ,  $\text{Fe}_3\text{O}_4$ ,  $\text{SiO}_2$  and N-coordinate ruthenium(II) arene complexes: multifunctional catalysts in the hydrogenation of nitroarenes and the transfer hydrogenation of aryl ketones, *Appl. Catal. B: Environ.* 164 (2015) 305–315.
- [3] S.K. Mohapatra, S.U. Sonavane, R.V. Jayaram, P. Selvam, Reductive cleavage of azo dyes and reduction of nitroarenes over trivalent iron incorporated hexagonal mesoporous aluminophosphate molecular sieves, *Appl. Catal. B: Environ.* 46 (2003) 155–163.
- [4] M. Boronat, P. Concepción, A. Corma, S. González, F. Illas, P. Serna, A molecular mechanism for the chemoselective hydrogenation of substituted nitroaromatics with nanoparticles of gold on  $\text{TiO}_2$  catalysts: a cooperative effect between gold and the support, *J. Am. Chem. Soc.* 129 (2007) 16230–16237.
- [5] J. Song, Z.-F. Huang, L. Pan, K. Li, X. Zhang, L. Wang, J.-J. Zou, Review on selective hydrogenation of nitroarene by catalytic, photocatalytic and electrocatalytic reactions, *Appl. Catal. B: Environ.* 227 (2018) 386–408.
- [6] R. Gao, L. Pan, H. Wang, X. Zhang, L. Wang, J.-J. Zou, Ultradispersed nickel phosphide on phosphorus-doped carbon with tailored d-band center for efficient and chemoselective hydrogenation of nitroarenes, *ACS Catal.* 8 (2018) 8420–8429.
- [7] M. Takasaki, Y. Motoyama, K. Higashi, S.-H. Yoon, I. Mochida, H. Nagashima, Chemoselective hydrogenation of nitroarenes with carbon nanofiber-supported platinum and palladium nanoparticles, *Org. Lett.* 10 (2008) 1601–1604.
- [8] K. Tsutsumi, F. Uchikawa, K. Sakai, K. Tabata, Photoinduced reduction of nitroarenes using a transition-metal-loaded silicon semiconductor under visible light irradiation, *ACS Catal.* 6 (2016) 4394–4398.
- [9] S. Fountoulaki, V. Daikopoulou, P.L. Gkizis, I. Tamiolakis, G.S. Armatas, I.N. Lykakis, Mechanistic studies of the reduction of nitroarenes by  $\text{NaBH}_4$  or hydrosilanes catalyzed by supported gold nanoparticles, *ACS Catal.* 4 (2014) 3504–3511.
- [10] K.-i. Shimizu, Y. Miyamoto, A. Satsuma, Size- and support-dependent silver cluster catalysis for chemoselective hydrogenation of nitroaromatics, *J. Catal.* 270 (2010) 86–94.
- [11] J. Song, Z.-F. Huang, L. Pan, J.-J. Zou, X. Zhang, L. Wang, Oxygen-deficient tungsten oxide as versatile and efficient hydrogenation catalyst, *ACS Catal.* 5 (2015) 6594–6599.
- [12] R. Gao, L. Pan, J. Lu, J. Xu, X. Zhang, L. Wang, J.-J. Zou, Phosphorus-doped and lattice-defective carbon as metal-like catalyst for the selective hydrogenation of nitroarenes, *ChemCatChem* 9 (2017) 4287–4294.
- [13] L. Li, L. Li, C. Cui, H. Fan, R. Wang, Heteroatom-doped carbon spheres from hierarchical hollow covalent organic framework precursors for metal-free catalysis, *ChemSusChem* (2017) 4921–4926.
- [14] B. List, Emil Knoevenagel and the roots of aminocatalysis, *Angew. Chem. Int. Ed.* 49 (2010) 1730–1734.
- [15] J. Gascon, U. Aktay, M.D. Hernandez-Alonso, G.P.M. van Klink, F. Kapteijn, Amino-based metal-organic frameworks as stable, highly active basic catalysts, *J. Catal.* 261 (2009) 75–87.
- [16] M.G. Álvarez, A.M. Frey, J.H. Bitter, A.M. Segarra, K.P. de Jong, F. Medina, On the role of the activation procedure of supported hydroxalcites for base catalyzed reactions: glycerol to glycerol carbonate and self-condensation of acetone, *Appl. Catal. B: Environ.* 134–135 (2013) 231–237.
- [17] B. Şen, E.H. Akdere, A. Şavk, E. Gültekin, Ö. Paralı, H. Göksu, F. Şen, A novel thiocarbamide functionalized graphene oxide supported bimetallic monodisperse Rh-Pt nanoparticles ( $\text{RhPt/TC@GO NPs}$ ) for Knoevenagel condensation of aryl aldehydes together with malononitrile, *Appl. Catal. B: Environ.* 225 (2018) 148–153.
- [18] C.I. Ezugwu, B. Mousavi, M.A. Asraf, Z. Luo, F. Verpoort, Post-synthetic modified MOF for Sonogashira cross-coupling and Knoevenagel condensation reactions, *J. Catal.* 344 (2016) 445–454.
- [19] B. Sakhivel, A. Dhakshinamoorthy, Chitosan as a reusable solid base catalyst for Knoevenagel condensation reaction, *J. Colloid Interface Sci.* 485 (2017) 75–80.
- [20] X. Li, B. Lin, H. Li, Q. Yu, Y. Ge, X. Jin, X. Liu, Y. Zhou, J. Xiao, Carbon doped hexagonal BN as a highly efficient metal-free base catalyst for Knoevenagel condensation reaction, *Appl. Catal. B: Environ.* 239 (2018) 254–259.
- [21] M.R. Benzigar, S.N. Talapaneni, S. Joseph, K. Ramadas, G. Singh, J. Scaranto, U. Ravon, K. Al-Bahily, A. Vinu, Recent advances in functionalized micro and mesoporous carbon materials: synthesis and applications, *Chem. Soc. Rev.* 47 (2018) 2680–2721.
- [22] H. Huang, X. Wang, Recent progress on carbon-based support materials for electrocatalysts of direct methanol fuel cells, *J. Mater. Chem. A* 2 (2014) 6266–6291.
- [23] W. Wu, Q. Zhang, X. Wang, C. Han, X. Shao, Y. Wang, J. Liu, Z. Li, X. Lu, M. Wu, Enhancing selective photooxidation through Co-Nx-doped carbon materials as singlet oxygen photosensitizers, *ACS Catal.* 7 (2017) 7267–7273.
- [24] L. Miao, D. Zhu, M. Liu, H. Duan, Z. Wang, Y. Lv, W. Xiong, Q. Zhu, L. Li, X. Chai, L. Gan, Cooking carbon with protic salt: nitrogen and sulfur self-doped porous carbon nanosheets for supercapacitors, *Chem. Eng. J.* 347 (2018) 233–242.
- [25] R. Gao, L. Pan, Z. Li, X. Zhang, L. Wang, J.-J. Zou, Cobalt nanoparticles encapsulated in nitrogen-doped carbon for room-temperature selective hydrogenation of nitroarenes, *Chin. J. Catal.* 39 (2018) 664–672.
- [26] T. Cheng, W. Hao-Fan, C. Xiang, L. Bo-Quan, H. Ting-Zheng, Z. Bingsen, Z. Qiang, T. Maria-Magdalena, W. Fei, Topological defects in metal-free nanocarbon for oxygen electrocatalysis, *Adv. Mater.* 28 (2016) 6845–6851.
- [27] L.-S. Marcos, P. Ana, G. Hermenegildo, P-doped graphene obtained by pyrolysis of modified alginate as a photocatalyst for hydrogen generation from water-methanol mixtures, *Angew. Chem. Int. Ed.* 52 (2013) 11813–11816.
- [28] F. Yang, C. Chi, C. Wang, Y. Wang, Y. Li, High graphite N content in nitrogen-doped graphene as an efficient metal-free catalyst for reduction of nitroarenes in water, *Green Chem.* 18 (2016) 4254–4262.
- [29] X.-k. Kong, Z.-y. Sun, M. Chen, C.-l. Chen, Q.-w. Chen, Metal-free catalytic reduction of 4-nitrophenol to 4-aminophenol by N-doped graphene, *Energy Environ. Sci.* 6 (2013) 3260.
- [30] S. Fujita, A. Katagiri, H. Watanabe, S. Asano, H. Yoshida, M. Arai, Preparation of nitrogen-doped carbon from polyacrylonitrile and its application as a solid-base catalyst, *ChemCatChem* 7 (2015) 2965–2970.
- [31] N.D. Shcherban, P. Mäki-Arvela, A. Aho, S.A. Sergienko, P.S. Yaremov, K. Eränen, D.Y. Murzin, Melamine-derived graphitic carbon nitride as a new effective metal-free catalyst for Knoevenagel condensation of benzaldehyde with ethylcyanoacetate, *Catal. Sci. Technol.* 8 (2018) 2928–2937.
- [32] Y. Liu, Z. Wang, W. Teng, H. Zhu, J. Wang, A.A. Elzatahry, D. Al-Dahyan, W. Li, Y. Deng, D. Zhao, A template-catalyzed in situ polymerization and co-assembly strategy for rich nitrogen-doped mesoporous carbon, *J. Mater. Chem. A* 6 (2018) 3162–3170.
- [33] R. Zhu, Q. Chen, X. Wang, S. Wang, J. Zhu, H. He, Templated synthesis of nitrogen-doped graphene-like carbon materials using spent montmorillonite, *RSC Adv.* 5 (2015) 7522–7528.
- [34] M. Li, F. Xu, H. Li, Y. Wang, Nitrogen-doped porous carbon materials: promising catalysts or catalyst supports for heterogeneous hydrogenation and oxidation, *Catal. Sci. Technol.* 6 (2016) 3670–3693.
- [35] Y. Deng, Y. Xie, K. Zou, X. Ji, Review on recent advances in nitrogen-doped carbons: preparations and applications in supercapacitors, *J. Mater. Chem. A* 4 (2016) 1144–1173.
- [36] H.-C. Ma, J.-L. Kan, G.-J. Chen, C.-X. Chen, Y.-B. Dong, Pd NPs-loaded homochiral covalent organic framework for heterogeneous asymmetric catalysis, *Chem. Mater.* 29 (2017) 6518–6524.
- [37] X. Guo, Y. Tian, M. Zhang, Y. Li, R. Wen, X. Li, X. Li, Y. Xue, L. Ma, C. Xia, S. Li, Mechanistic insight into hydrogen-bond-controlled crystallinity and adsorption property of covalent organic frameworks from flexible building blocks, *Chem. Mater.* (2018) 2299–2308.
- [38] Z. Li, Y. Zhi, X. Feng, X. Ding, Y. Zou, X. Liu, Y. Mu, An azine-linked covalent organic framework: synthesis, characterization and efficient gas storage, *Chem. Eur. J.* 21 (2015) 12079–12084.
- [39] L. Li, L. Li, C. Cui, H. Fan, R. Wang, Heteroatom-doped carbon spheres from hierarchical hollow covalent organic framework precursors for metal-free catalysis, *ChemSusChem* 10 (2017) 4921–4926.
- [40] Q. Xu, Y. Tang, X. Zhang, Y. Oshima, Q. Chen, D. Jiang, Template conversion of covalent organic frameworks into 2D conducting nanocarbons for catalyzing oxygen reduction reaction, *Adv. Mater.* 30 (2018) 1706330.
- [41] H. Wang, C. Wang, Y. Yang, M. Zhao, Y. Wang,  $\text{H}_3\text{PW}_{12}\text{O}_{40}/\text{mpg-C}_3\text{N}_4$  as an efficient and reusable bifunctional catalyst in one-pot oxidation-Knoevenagel condensation tandem reaction, *Catal. Sci. Technol.* 7 (2017) 405–417.
- [42] A.K. Fine, M.P. Schmidt, C.E. Martinez, Nitrogen-rich compounds constitute an increasing proportion of organic matter with depth in O-i-O-e-O-a-A horizons of temperate forests, *Geoderma* 323 (2018) 1–12.
- [43] H. Dong, X. Guo, C. Yang, Z. Ouyang, Synthesis of g- $\text{C}_3\text{N}_4$  by different precursors under burning explosion effect and its photocatalytic degradation for tylosin, *Appl. Catal. B: Environ.* 230 (2018) 65–76.
- [44] M. Faisal, A.A. Ismail, F.A. Harraz, S.A. Al-Sayari, A.M. El-Toni, M.S. Al-Assiri, Synthesis of highly dispersed silver doped g- $\text{C}_3\text{N}_4$  nanocomposites with enhanced visible-light photocatalytic activity, *Mater. Design* 98 (2016) 223–230.
- [45] Y. Leng, J. Li, C. Zhang, P. Jiang, Y. Li, Y. Jiang, S. Du, N-Doped carbon encapsulated molybdenum carbide as an efficient catalyst for oxidant-free dehydrogenation of alcohols, *J. Mater. Chem. A* 5 (2017) 17580–17588.
- [46] X. Cui, H. Li, M. Yuan, J. Yang, D. Xu, Z. Li, G. Yu, Y. Hou, Z. Dong, Facile preparation of fluffy N-doped carbon modified with Ag nanoparticles as a highly active and reusable catalyst for catalytic reduction of nitroarenes, *J. Colloid Interface Sci.* 506 (2017) 524–531.
- [47] R. Li, A. Cao, Y. Zhang, G. Li, F. Jiang, S. Li, D. Chen, C. Wang, J. Ge, C. Shu, Formation of nitrogen-doped mesoporous graphitic carbon with the help of melamine, *ACS Appl. Mater. Interfaces* 6 (2014) 20574–20578.
- [48] Z. Xie, Z. He, X. Feng, W. Xu, X. Cui, J. Zhang, C. Yan, M.A. Carreon, Z. Liu, Y. Wang, Hierarchical sandwich-like structure of ultrafine N-rich porous carbon nanospheres grown on graphene sheets as superior lithium-ion battery anodes, *ACS Appl. Mater. Interfaces* 8 (2016) 10324–10333.
- [49] Y. Zhang, Y. Ma, Y.-Y. Chen, L. Zhao, L.-B. Huang, H. Luo, W.-J. Jiang, X. Zhang, S. Niu, D. Gao, J. Bi, G. Fan, J.-S. Hu, Encased copper boosts the electrocatalytic activity of N-doped carbon nanotubes for hydrogen evolution, *ACS Appl. Mater. Interfaces* 9 (2017) 36857–36864.
- [50] X. Cui, Y. Long, X. Zhou, G. Yu, J. Yang, M. Yuan, J. Ma, Z. Dong, Pd-doped Ni nanoparticle-modified N-doped carbon nanocatalyst with high Pd atom utilization for the transfer hydrogenation of nitroarenes, *Green Chem.* 20 (2018) 1121–1130.
- [51] G. Sarau, M. Heilmann, M. Bashouti, M. Latzel, C. Tessarek, S. Christiansen, Efficient nitrogen doping of single-layer graphene accompanied by negligible defect generation for integration into hybrid semiconductor heterostructures, *ACS Appl. Mater. Interfaces* 9 (2017) 10003–10011.
- [52] L.-H. Liu, M. Yan, Perfluorophenyl azides: new applications in surface functionalization and nanomaterial synthesis, *Acc. Chem. Res.* 43 (2010) 1434–1443.
- [53] Y. Gao, G. Hu, J. Zhong, Z. Shi, Y. Zhu, D.S. Su, J. Wang, X. Bao, D. Ma, Nitrogen-doped sp<sup>2</sup>-hybridized carbon as a superior catalyst for selective oxidation, *Angew. Chem. Int. Ed.* 52 (2013) 2109–2113.
- [54] L. Yang, W.A. Yee, S.L. Phua, J. Kong, H. Ding, J.W. Cheah, X. Lu, A high throughput method for preparation of highly conductive functionalized graphene and conductive polymer nanocomposites, *RSC Adv.* 2 (2012) 2208.
- [55] A.L. Cazetta, T. Zhang, T.L. Silva, V.C. Almeida, T. Asefa, Bone char-derived metal-free N- and S-co-doped nanoporous carbon and its efficient electrocatalytic activity for hydrazine oxidation, *Appl. Catal. B: Environ.* 225 (2018) 30–39.

- [56] J. Gong, J. Liu, X. Chen, Z. Jiang, X. Wen, E. Mijowska, T. Tang, Converting real-world mixed waste plastics into porous carbon nanosheets with excellent performance in the adsorption of an organic dye from wastewater, *J. Mater. Chem. A* 3 (2015) 341–351.
- [57] L.J. Konwar, P. Mäki-Arvela, E. Salminen, N. Kumar, A.J. Thakur, J.-P. Mikkola, D. Deka, Towards carbon efficient biorefining: multifunctional mesoporous solid acids obtained from biodiesel production wastes for biomass conversion, *Appl. Catal. B: Environ.* 176–177 (2015) 20–35.
- [58] Z.-H. Sheng, L. Shao, J.-J. Chen, W.-J. Bao, F.-B. Wang, X.-H. Xia, Catalyst-free synthesis of nitrogen-doped graphene via thermal annealing graphite oxide with melamine and its excellent electrocatalysis, *ACS Nano* 5 (2011) 4350–4358.
- [59] J. Wu, Z. Pan, Y. Zhang, B. Wang, H. Peng, The recent progress of nitrogen-doped carbon nanomaterials for electrochemical batteries, *J. Mater. Chem. A* 6 (2018) 12932–12944.
- [60] M. Mananghaya, E. Rodulfo, G.N. Santos, A.R. Villagracia, A.N. Ladines, Theoretical investigation on single-wall carbon nanotubes doped with nitrogen, pyridine-like nitrogen defects, and transition metal atoms, *J. Nanomat.* (2012) (2012) 1–14.
- [61] F. Cárdenas-Lizana, S. Gómez-Quero, G. Jacobs, Y. Ji, B.H. Davis, L. Kiwi-Minsker, M.A. Keane, Alumina supported Au–Ni: surface synergism in the gas phase hydrogenation of nitro-compounds, *J. Phys. Chem. C* 116 (2012) 11166–11180.
- [62] X. Wang, F. Cárdenas-Lizana, M.A. Keane, Toward sustainable chemoselective nitroarene hydrogenation using supported gold as catalyst, *ACS Sustain. Chem. Eng.* 2 (2014) 2781–2789.
- [63] S. Cai, H. Duan, H. Rong, D. Wang, L. Li, W. He, Y. Li, Highly active and selective catalysis of bimetallic Rh3Ni1 nanoparticles in the hydrogenation of nitroarenes, *ACS Catal.* 3 (2013) 608–612.
- [64] T.C. Araújo, Hd.S. Oliveira, J.J.S. Teles, J.D. Fabris, L.C.A. Oliveira, J.P. de Mesquita, Hybrid heterostructures based on hematite and highly hydrophilic carbon dots with photocatalytic activity, *Appl. Catal. B: Environ.* 182 (2016) 204–212.
- [65] P. Zhang, Y. Hu, B. Li, Q. Zhang, C. Zhou, H. Yu, X. Zhang, L. Chen, B. Eichhorn, S. Zhou, Kinetically stabilized Pd@Pt core–shell octahedral nanoparticles with thin Pt layers for enhanced catalytic hydrogenation performance, *ACS Catal.* 5 (2015) 1335–1343.
- [66] H. Liu, K. Tao, C. Xiong, S. Zhou, Controlled synthesis of Pd–NiO@SiO<sub>2</sub> mesoporous core–shell nanoparticles and their enhanced catalytic performance for p-chloronitrobenzene hydrogenation with H<sub>2</sub>, *Catal. Sci. Technol.* 5 (2015) 405–414.